Journal of Alloys and Compounds 518 (2012) 51–57

Contents lists available at SciVerse ScienceDirect

Journal of Alloys and Compounds

journal homepage: www.elsevier.com/locate/jallcom

Multiferroic properties in $BiFe_{1-x}Zn_xO_3$ ($x = 0.1–0.2$) ceramics by solution combustion method (SCM)

Y.A. Chaudhari[a], A. Singh[b], E.M. Abuassaj[a], R. Chatterjee[b], S.T. Bendre[a,*]

[a] Department of Physics, School of Physical Sciences, North Maharashtra University, Jalgaon 425 001 (M.S.), India
[b] Magnetics and Advanced Ceramics Laboratory, Indian Institute of Technology Delhi, Hauz Khas, New Delhi 110 016, India

ARTICLE INFO

Article history:
Received 28 September 2011
Received in revised form
22 December 2011
Accepted 23 December 2011
Available online 30 December 2011

Keywords:
$BiFe_{1-x}Zn_xO_3$ ($x = 0.1–0.2$) ceramics
Solution combustion method
Characterizations
Multiferroic properties

ABSTRACT

Multiferroic $BiFe_{1-x}Zn_xO_3$ ($x = 0$, 0.1, 0.15, and 0.2) ceramics were prepared by solution combustion method (SCM). The room temperature ferroelectric and magnetic hysteresis loops shows coexistence of magnetism and ferroelectricity. It was found that room temperature magnetization measurement gives rise to the appearance of weak ferromagnetism and exhibits a superparamagnetic nature at 5 K in $BiFe_{1-x}Zn_xO_3$ ($x = 0.1–0.2$) ceramics. The ferroelectric hysteresis loops measured at room temperature. It shows the unsaturated behavior which indicates the partial reversal of polarization. A dielectric constant with temperature measurement in $BiFe_{0.9}Zn_{0.1}O_3$ and $BiFe_{0.85}Zn_{0.15}O_3$ samples exhibits an apparent dielectric anomaly around 350 and 300 °C and demonstrates an antiferromagnetic to paramagnetic phase transition (T_N) of $BiFeO_3$. The structural study was carried out using X-ray diffraction (XRD) pattern and showed that $BiFe_{1-x}Zn_xO_3$ ($x = 0.1–0.2$) ceramics have rhombhohedral perovskite structure and surface morphology of the samples were examined by scanning electron microscope (SEM).

1. Introduction

Multiferroic material exhibits an electric and magnetic nature mutually which results in communal existence of ferroelectricity and ferromagnetism in a single phase [1]. Due to the coupling between electric and magnetic ordered parameters, it generates a novel phenomena known as magnetoelectric effect (ME) in which polarization can be switched by applied magnetic field and vice versa. Particularly, it provides an additional opportunities for the fabrication of microelectronic and spintronic devices [2–4]. These materials have an enormous attention towards their potential applications in various fields, such as information storage, spintronic, sensors [5], thin film capacitor, nonvolatile memory, nonlinear optics, photoelectrochemical cell, magnetoelectric sensor devices, multiple state memories, high density ferroelectric random access memory, electric field controlled ferromagnetic resonance devices, radio transmission, microwave as well as satellite communication, digital recording, and permanent magnet applications [6–10]. The perovskite $BiFeO_3$ is one of the multifunctional material which shows magnetoelectric coupling at room temperature having relatively high ferroelectric Curie temperature $T_C \sim 1103$ K and Neel temperature $T_N \sim 643$ K [11–13].

Intended for admirations, many co-workers are engaged towards the improvement in ferroelectric and dielectric properties of topical material, such as $BiFeO_3$, using various trivalent dopants, such as Mn [5], Ba [14], La [15], Cr [16], Ti [17], Sm [18]. In this anxiety, an early study showed that the ferroelectricity and magnetization in $BiFeO_3$ based on divalent dopants. Among this, the magnetic properties of Zn doped $BiFeO_3$ ceramics using rapid sintering method also shows the clear magnetic hysteresis loop at room temperature with significantly improved dielectric properties by Xu et al. [19]. Enhanced magnetic properties of Ni doped $BiFeO_3$ at doping concentration of 0.5% using hydrothermal route was observed by Wang et al. [20]. Also, the multiferroic properties of solid state synthesized $Bi_{1-x}Ca_xFeO_3$ system and proved the leakage current increases with increment in Ca doping by Kothari et al. [21]. Recently, Chen et al. have reported the multiferroic properties of rapid thermal synthesized $Bi_{1-x}Ca_xFeO_3$ ceramics, highly resistive hysteresis loops and improved magnetic properties with suppressed spin modulated structure [22].

To the best of our knowledge no any single report is present on $BiFe_{1-x}Zn_xO_3$ using solution combustion route and their multiferroic properties of Zn doped $BiFeO_3$. Amid this vision, in present paper we report the preparation of $BiFe_{1-x}Zn_xO_3$ compound using solution combustion route and the results could help towards the enhancement in electric, magnetic, and dielectric properties in Zn doped $BiFeO_3$.

* Corresponding author. Tel.: +91 257 2257478; fax: +91 257 2258403.
E-mail address: bendrest@gmail.com (S.T. Bendre).

0925-8388/$ – see front matter © 2011 Elsevier B.V. All rights reserved.
doi:10.1016/j.jallcom.2011.12.122

2. Experimental

2.1. Materials

For the preparation of $BiFe_{1-x}Zn_xO_3$ ($x = 0$, 0.1, 0.15, and 0.2) ceramics the precursors, such as $Bi(NO_3)_3{\cdot}5H_2O$ (CDH, India), $Fe(NO_3)_3{\cdot}9H_2O$ (Fischer Scientific), $Zn(NO_3)_2{\cdot}6H_2O$ (CDH, India), were used as oxidizers whereas glycine (NH_2CH_2COOH) (CDH, India) was used as a fuel.

2.2. Synthesis process of $BiFe_{1-x}Zn_xO_3$

The $BiFe_{1-x}Zn_xO_3$ ($x = 0$, 0.1, 0.15, and 0.2) multiferroic ceramics were prepared by solution combustion method (SCM). For this, the oxidizer (O): fuel (F) ratio was calculated on the basis of oxidizing valencies of metal nitrates and reducing valency of fuel [23]. The above mentioned metal nitrates and glycine in stiochiometric ratios were completely dissolved in distilled water. Afterward, the mixture was heated in a Pyrex dish (150 × 50 mm) on a burner until the excess of free water evaporates and at the same time spontaneous ignition occurred; thereafter a combustion powders were obtained. These powders of pure $BiFeO_3$, different concentrations of Zn doped compositions were grinded and calcinated at 650 °C for 4 h. In addition, these powders were pelletized under uniaxial pressing through addition of polyvinyl alcohol as a binder. Lastly, these pellets are sintered at different temperatures as 670 °C ($x = 0.0$), 675 °C ($x = 0.1$), 680 °C ($x = 0.15$), and 685 °C ($x = 0.2$) for 30 min and used for further experimental measurements

2.3. Characterization

The sintered samples were characterized by X-ray diffraction (XRD) using CuKα1 radiation (λ = 1.54178 Å) (Philips X-pert PRO) for phase identification in the 2θ range (20–75°). The surface morphology of the $BiFe_{1-x}Zn_xO_3$ ($x = 0.0$, 0.1, 0.15, and 0.2) compound was examined by scanning electron microscope (SEM, EVO-50). Dielectric measurement was done on H.P. Impedance analyzer (4192A LF) in the frequency range of 10 kHz–1 MHz with varying temperature from 30 to 400 °C. The dielectric constant as a function of frequency was measured by Precision Impedance analyzer (Agilent 4294A) at room temperature. The ferroelectric measurement was carried out at room temperature on ferroelectric tester (Radiant Precision Premier II Technology) at 10 kHz. For electrical characterizations, an Ag paste was enforced to both sides of the sintered pellets. A superconducting quantum interface device (SQUID) (Quantum Design, MPMS-7) system was used to measure the field dependence magnetization of the ceramics.

3. Results and discussion

3.1. Structural studies

Fig. 1(a)–(c) shows the RT X-ray diffraction patterns of $BiFe_{0.9}Zn_{0.1}O_3$, $BiFe_{0.85}Zn_{0.15}O_3$, and $BiFe_{0.8}Zn_{0.2}O_3$ samples. The XRD result reveals that the Zn doped $BiFeO_3$ samples have rhombhohedral perovskite structure. The Zn doping concentration is varied from 0.1 to 0.2 thereafter, the additional impurity phase $Bi_{12}(Bi_{0.5}Fe_{0.5})O_{19.5}$ have been observed in the samples around 30° in 2θ range. The XRD pattern is well accorded with reported results by Xu et al. [19]. According to the above results, it is observed that Zn ions are effectively incorporated into the crystal structure of $BiFeO_3$. Since, it is a great challenge to prepare pure $BiFeO_3$ as the product; because it mainly, contaminated with secondary phases of Bi_2O_3 and $Bi_2Fe_4O_9$ [24]. The average crystallite size was calculated by using Scherrer's formula:

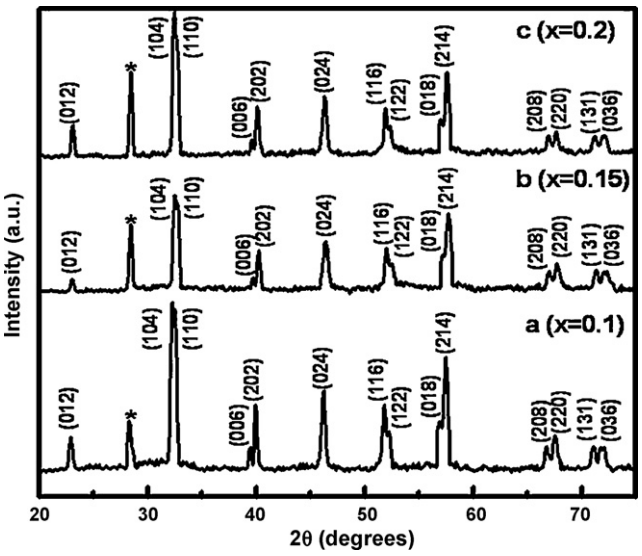

Fig. 1. X-ray diffraction (XRD) patterns of (a) $BiFe_{0.9}Zn_{0.1}O_3$ sintered at 675 °C for 30 min, (b) $BiFe_{0.85}Zn_{0.15}O_3$ sintered at 680 °C for 30 min, and (c) $BiFe_{0.8}Zn_{0.2}O_3$ sintered at 685 °C for 30 min, obtained by SCM.

$$t = \frac{k\lambda}{\beta\cos(\theta)}$$

where 't' is the crystal size; 'λ' is the wavelength of X-ray used; 'β' is the angular line width of half maximum intensity; and 'θ' is the Bragg's angle. The calculated average crystallite size of $BiFe_{0.9}Zn_{0.1}O_3$, $BiFe_{0.85}Zn_{0.15}O_3$, and $BiFe_{0.8}Zn_{0.2}O_3$ ceramics were found to be 20.84 nm, 21.96 nm, and 18.95 nm respectively.

3.2. Surface morphology

Fig. 2(a)–(c) presents the microstructure of the $BiFe_{0.9}Zn_{0.1}O_3$, $BiFe_{0.85}Zn_{0.15}O_3$, and $BiFe_{0.8}Zn_{0.2}O_3$ sintered samples. The surface morphologies of doped ceramics were dense and no segregation of Zn at grain boundary was observed. It can be observed with increasing Zn dopants; the particles are agglomerated with interconnected structure and grain size of BFZO ceramics was reduced and uniformly distributed over the surface.

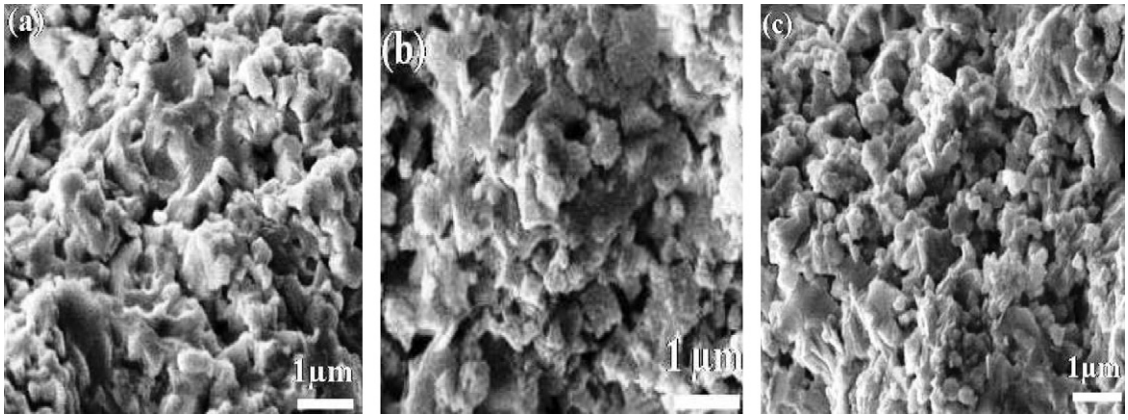

Fig. 2. Scanning electron micrographs of (a) $BiFeO_3$, (b) $BiFe_{0.9}Zn_{0.1}O_3$, (c) $BiFe_{0.85}Zn_{0.15}O_3$ sintered at 680 °C for 30 min, and (d) $BiFe_{0.8}Zn_{0.2}O_3$ sintered at 685 °C for 30 min.

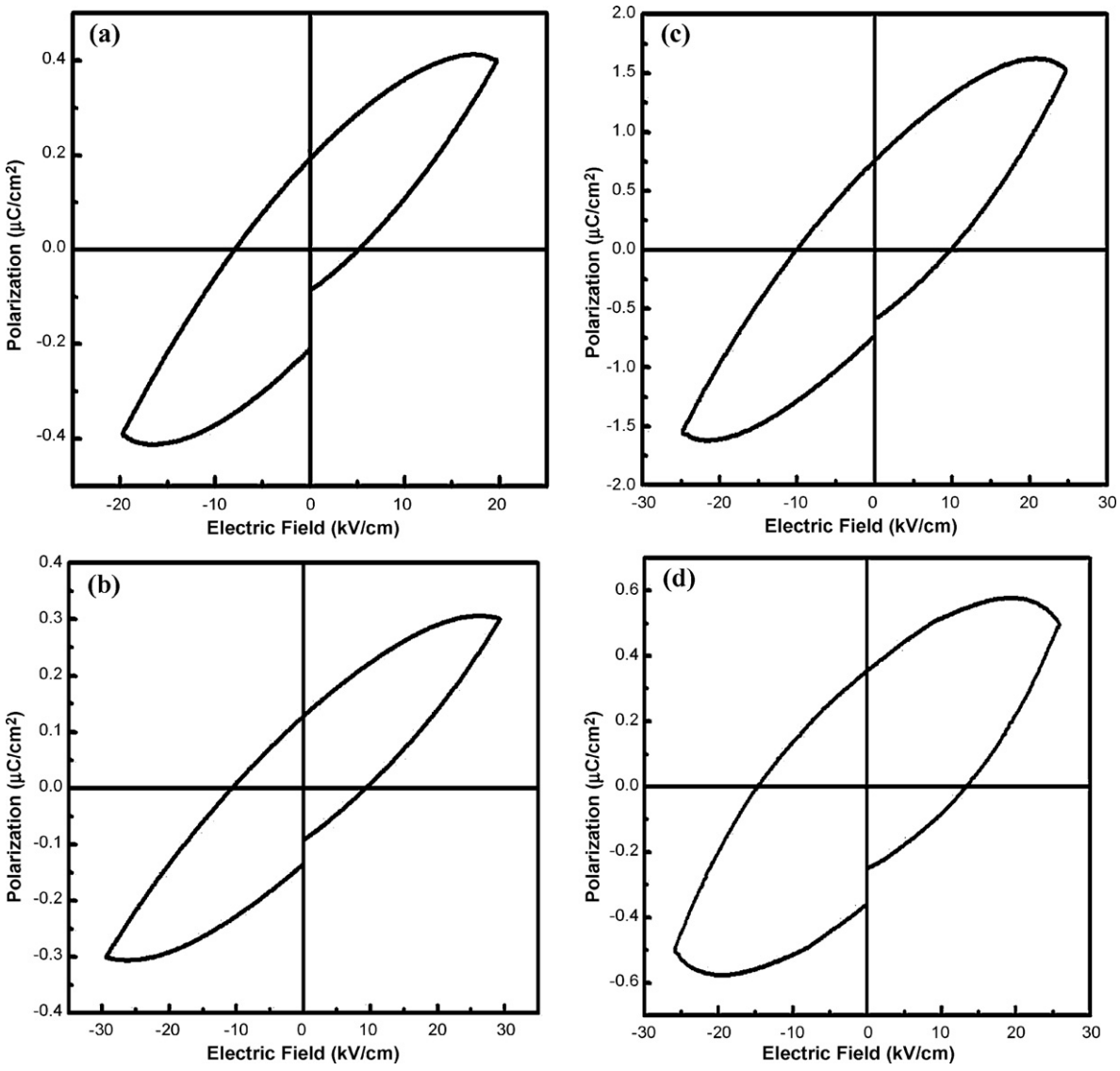

Fig. 3. Room temperature (RT) P–E hysteresis loops at f = 10 kHz for (a) $BiFeO_3$, (b) $BiFe_{0.9}Zn_{0.1}O_3$, (c) $BiFe_{0.85}Zn_{0.15}O_3$, and (d) $BiFe_{0.8}Zn_{0.2}O_3$ samples.

3.3. Ferroelectric P–E hysteresis loops

Fig. 3(a)–(d) illustrates the P–E hysteresis loops of $BiFeO_3$, $BiFe_{0.9}Zn_{0.1}O_3$, $BiFe_{0.85}Zn_{0.15}O_3$, and $BiFe_{0.8}Zn_{0.2}O_3$ ceramics sintered at 670, 675, 680, and 685 °C for 30 min. The ferroelectric (P–E) loops were measured at room temperature, at maximum electric field (E_m) of ±30 kV/cm. The loop seems to be unsaturated behavior because of higher leakage current and partial reversal of polarization. These leakage current values were observed due to increasing Zn doping concentration and charge neutralization of Zn^{2+} doping at Fe^{3+} site. Hence, it could be resulted into the higher leakage current in $BiFe_{1-x}Zn_xO_3$ (x = 0.1–0.2) compound. The P–E hysteresis loops of all samples indicate their ferroelectric behavior; due to changing Zn substitution level and the increase in lattice parameters of unit cell. Since the ionic radius of Zn^{2+} is slightly larger than that of Fe^{3+} and the enhancement in both "a" and "c" parameters were observed. Furthermore, the c/a ratio and Zn substitutions should not affect the crystalline structure of the parent compound $BiFeO_3$ as shown in Fig. 1(a)–(c). This could be crucial for enduring the ferroelectric properties in $BiFeO_3$ and $BiFe_{1-x}ZnO_3$ (x = 0.1–0.2) ceramics.

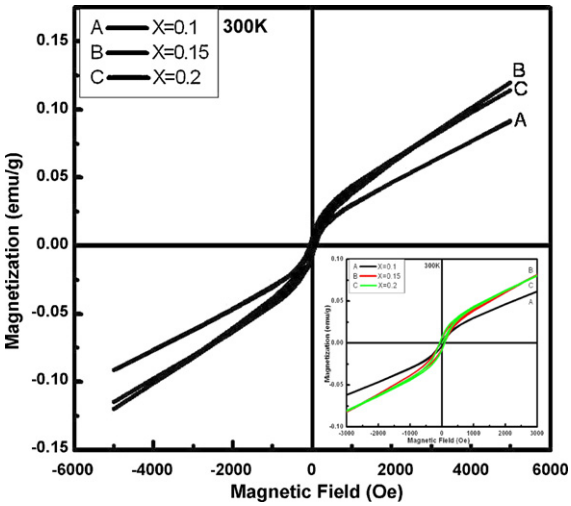

Fig. 4. Room temperature M–H loops under the applied magnetic field of 5 kOe for (A) $BiFe_{0.9}Zn_{0.1}O_3$, (B) $BiFe_{0.85}Zn_{0.15}O_3$, and (C) $BiFe_{0.8}Zn_{0.2}O_3$ samples. Inset shows low field M–H data at 3 kOe for (A) $BiFe_{0.9}Zn_{0.1}O_3$, (B) $BiFe_{0.85}Zn_{0.15}O_3$, and (C) $BiFe_{0.8}Zn_{0.2}O_3$ samples.

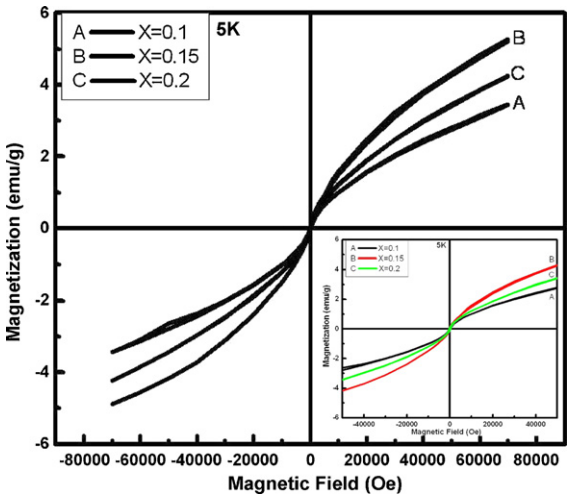

Fig. 5. Magnetic hysteresis (M–H) loops at 5 K under the applied field of 70 kOe for (A) $BiFe_{0.9}Zn_{0.1}O_3$, (B) $BiFe_{0.85}Zn_{0.15}O_3$, and (C) $BiFe_{0.8}Zn_{0.2}O_3$ samples. Inset shows low field M–H data at 50 kOe for (A) $BiFe_{0.9}Zn_{0.1}O_3$, (B) $BiFe_{0.85}Zn_{0.15}O_3$, and (C) $BiFe_{0.8}Zn_{0.2}O_3$ samples.

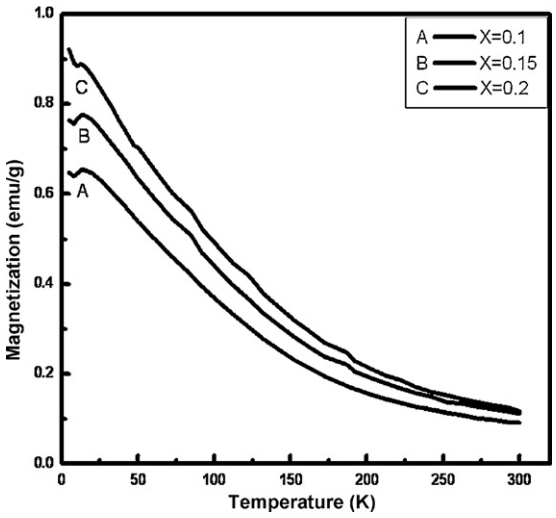

Fig. 6. M–T curve under magnetic field of 5000 Oe for (A) $BiFe_{0.9}Zn_{0.1}O_3$, (B) $BiFe_{0.85}Zn_{0.15}O_3$, and (C) $BiFe_{0.8}Zn_{0.2}O_3$ samples.

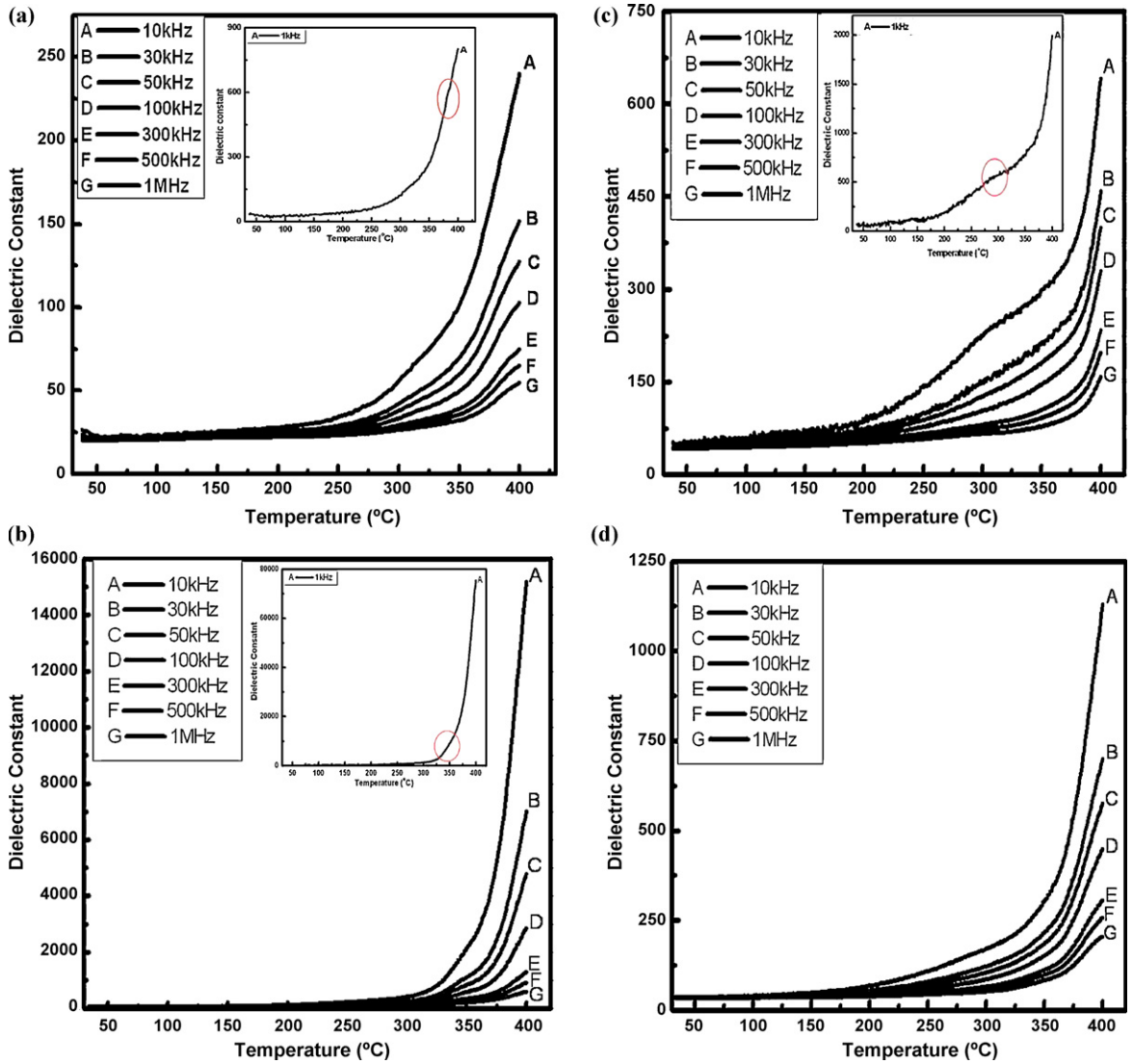

Fig. 7. Dielectric constant versus temperature measurements in the frequency range 1 kHz–1 MHz for (a) $BiFeO_3$ (curves A–G), inset shows ε–T plot of $BiFeO_3$ at 1 kHz (curve A); (b) $BiFe_{0.9}Zn_{0.1}O_3$ (curves A–G), inset shows ε–T plot of $BiFe_{0.9}Zn_{0.1}O_3$ at 1 kHz (curve A); (c) $BiFe_{0.85}Zn_{0.15}O_3$ (curves A–G), inset shows ε–T plot of $BiFe_{0.85}Zn_{0.15}O_3$ at 1 kHz (curve A); and (d) $BiFe_{0.8}Zn_{0.2}O_3$ (curves A–G) samples.

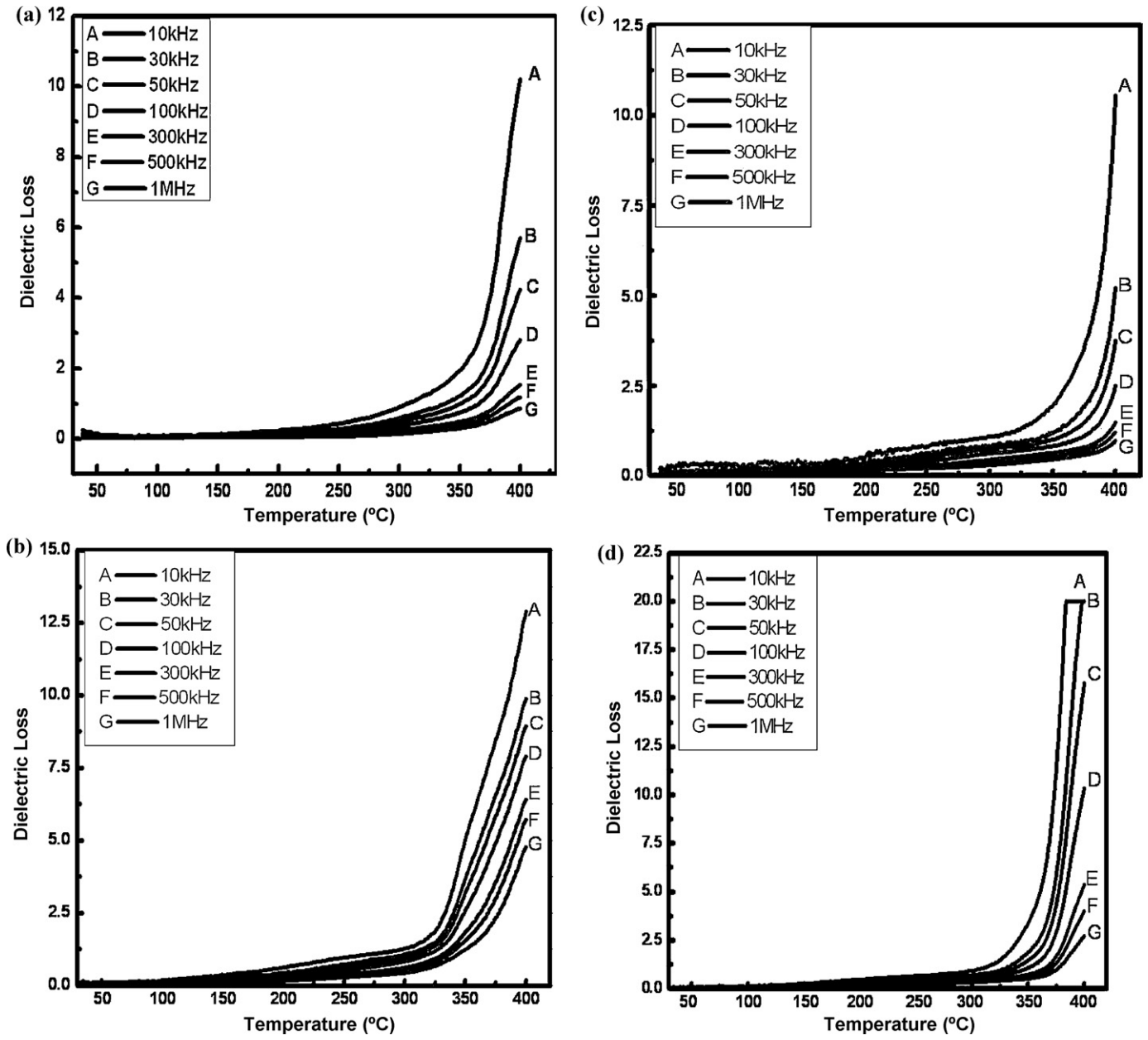

Fig. 8. Dielectric loss versus temperature measurements in the frequency range 10 kHz–1 MHz for (a) $BiFeO_3$ (curves A–G), (b) $BiFe_{0.9}Zn_{0.1}O_3$ (curves A–G), (c) $BiFe_{0.85}Zn_{0.15}O_3$ (curves A–G), and (d) $BiFe_{0.8}Zn_{0.2}O_3$ (curves A–G) samples.

3.4. Magnetic hysteresis (M–H) loops

In Fig. 4 the curves (A), (B), and (C) displayed the room temperature magnetic hysteresis loops of $BiFe_{0.9}Zn_{0.1}O_3$, $BiFe_{0.85}Zn_{0.15}O_3$, and $BiFe_{0.8}Zn_{0.2}O_3$ samples, respectively. The M–H dependencies of Zn^{2+} substituted $BiFeO_3$ compound have a linear character up to 5kOe; therefore confirming the weak ferromagnetism nature of $BiFe_{1-x}Zn_xO_3$ ($x = 0.1–0.2$) samples at 300 K. The values of coercive field for $BiFe_{0.9}Zn_{0.1}O_3$, $BiFe_{0.85}Zn_{0.15}O_3$, and $BiFe_{0.8}Zn_{0.2}O_3$ ceramics are 51, 74, and 83 Oe, respectively at 300 K. The curves (A), (B), and (C) with low field M–H data up to 3 kOe for $BiFe_{1-x}Zn_xO_3$ ($x = 0.1–0.2$) ceramics at 300 K are as depicted in inset of Fig. 4. Khomchenko et al. have studied the linear dependence of M–H for $Bi_{0.8}Ca_{0.2}FeO_3$ ceramics suggesting that Ca^{2+} is less effective in suppressing the spin cycloid [25].

At 5 K the magnetization measurements of $BiFe_{0.9}Zn_{0.1}O_3$, $BiFe_{0.85}Zn_{0.15}O_3$, and $BiFe_{0.8}Zn_{0.2}O_3$ ceramics as a function of the applied magnetic field corresponding to the curves (A), (B), and (C), respectively, are as shown in Fig. 5. The M–H hysteresis loops exhibit a superparamagnetic nature and present unsaturated loops for $BiFe_{0.9}Zn_{0.1}O_3$, $BiFe_{0.85}Zn_{0.15}O_3$, and $BiFe_{0.8}Zn_{0.2}O_3$ ceramics. The measured values of coercive field for $BiFe_{0.9}Zn_{0.1}O_3$, $BiFe_{0.85}Zn_{0.15}O_3$, and $BiFe_{0.8}Zn_{0.2}O_3$ ceramics are 299, 314, and 334 Oe respectively, at 5 K. The curves (A), (B), and (C) describe the low field M–H data up to 50 kOe for $BiFe_{1-x}Zn_xO_3$ ($x = 0.1–0.2$) ceramics at 5 K in inset of Fig. 5.

In Fig. 6 curves (A), (B), and (C) demonstrate the temperature dependence of magnetization for $BiFe_{0.9}Zn_{0.1}O_3$, $BiFe_{0.85}Zn_{0.15}O_3$, and $BiFe_{0.8}Zn_{0.2}O_3$ samples at 5 K with applied field of 50 kOe.

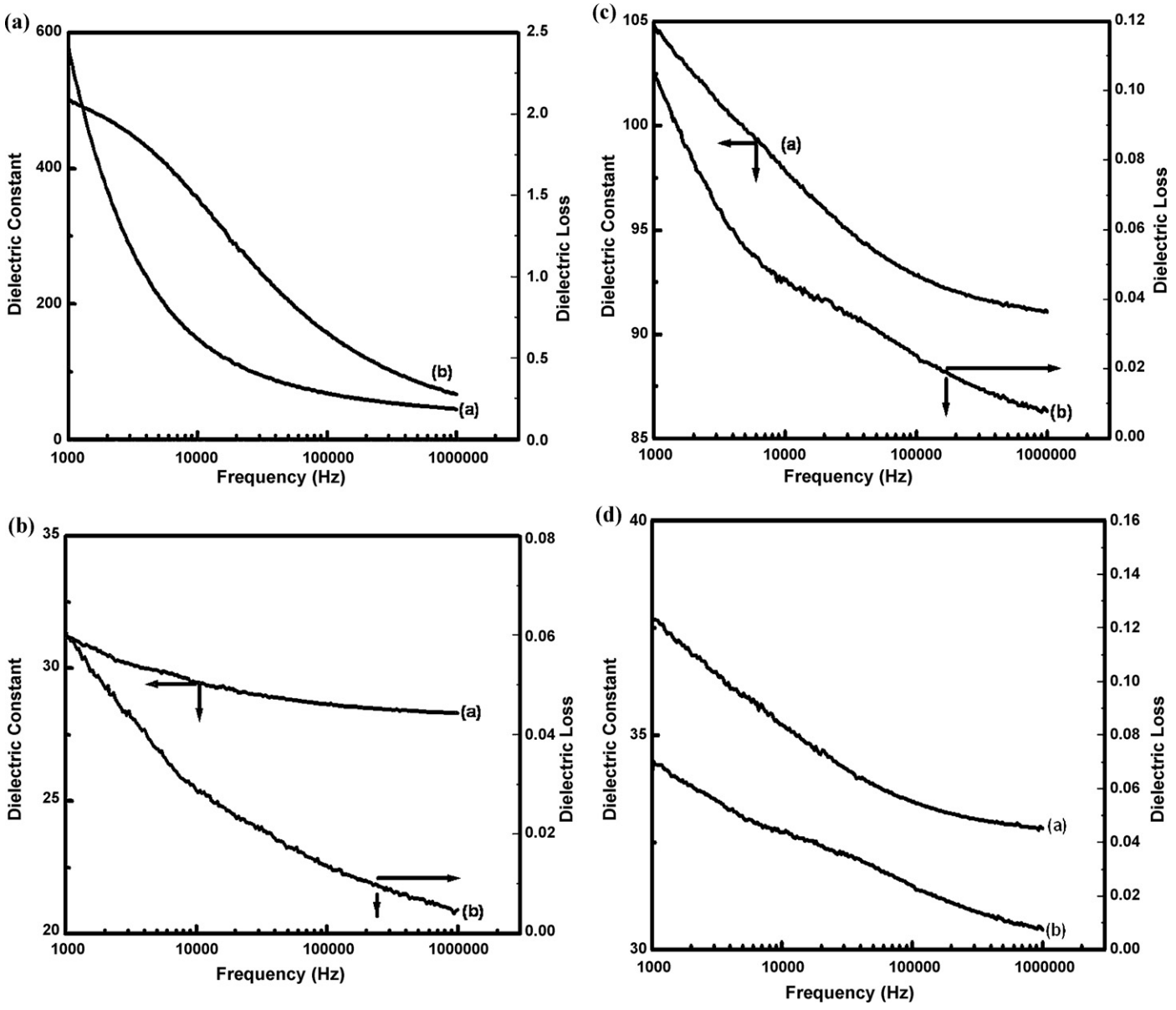

Fig. 9. Dielectric constant and loss versus frequency measurement at RT of (A) $BiFeO_3$ [dielectric constant curve (a) and loss curve (b)], (B) $BiFe_{0.9}Zn_{0.1}O_3$ [dielectric constant curve (a) and loss curve (b)], (C) $BiFe_{0.85}Zn_{0.15}O_3$ [dielectric constant curve (a) and loss curve (b)], and (D) $BiFe_{0.8}Zn_{0.2}O_3$ [dielectric constant curve (a) and loss curve (b)].

The magnetization decreases with increasing temperature for this $BiFe_{1-x}Zn_xO_3$ (0.1–0.2) system.

3.5. Dielectric measurements

Fig. 7(a)–(d) presents the temperature dependence of dielectric constant for $BiFeO_3$, $BiFe_{0.9}Zn_{0.1}O_3$, $BiFe_{0.85}Zn_{0.15}O_3$, and $BiFe_{0.8}Zn_{0.2}O_3$ ceramics. The frequency was varied from $f = 1$ kHz to 1 MHz. The dielectric constant shows the continuous increase with temperature for $BiFe_{1-x}Zn_xO_3$ ($x = 0.0$–0.2) system. A clear dielectric anomaly has been observed in $BiFeO_3$, $BiFe_{0.9}Zn_{0.1}0_3$, and $BiFe_{0.85}Zn_{0.15}O_3$ samples around 370, 350, and 300 °C. This anomaly seems to be related with phase transformation from antiferromagnetic to paramagnetic phase and manifests a possible coupling between electric and magnetic dipole moments in $BiFeO_3$ [26]. It can be observed that from Fig. 7(a)–(c) this anomaly shifted towards lower temperature with increasing Zn doping level in $BiFeO_3$. Similar results are also reported by Kumar et al. [5]. The inset of Fig. 7(a)–(c) shows dielectric constant as a function of temperature for $BiFe_{0.9}Zn_{0.1}O_3$ and $BiFe_{0.85}Zn_{0.15}O_3$ samples exhibits a similar dielectric anomaly around 370, 350, and 300 °C at 1 kHz. The room temperature values of dielectric constant for $BiFeO_3$, $BiFe_{0.9}Zn_{0.1}O_3$, $BiFe_{0.85}Zn_{0.15}O_3$, and $BiFe_{0.8}Zn_{0.2}O_3$ ceramics were 30, 52, 51, and 34, respectively.

The variation of dielectric loss ($\tan\delta$) with temperature is shown in Fig. 8(a)–(d) for $BiFeO_3$, $BiFe_{0.9}Zn_{0.1}O_3$, $BiFe_{0.85}Zn_{0.15}O_3$, and $BiFe_{0.8}Zn_{0.2}O_3$ ceramics. The frequency was varied from 10 kHz to 1 MHz. The dielectric loss shows a continuous increase with temperature. The room temperature values of dielectric loss for $BiFeO_3$, $BiFe_{0.9}Zn_{0.1}O_3$, $BiFe_{0.85}Zn_{0.15}O_3$, and $BiFe_{0.8}Zn_{0.2}O_3$ ceramics were 0.24, 0.12, 0.18, and 0.058, respectively. The frequency dependence of dielectric constant and dielectric loss measured in pure and Zn substituted $BiFeO_3$ ceramics at room temperature in the frequency range of 1 kHz–1 MHz is shown in Fig. 9(A)–(D) for $BiFe_{1-x}Zn_xO_3$ ($x = 0.0$–0.2). In the low frequency range, both "ε" and "$\tan\delta$" have very high values. It is evident that both "ε" and "$\tan\delta$" decrease gradually with the increase in frequency.

4. Conclusions

We have synthesized $BiFe_{1-x}Zn_xO_3$ ($x = 0, 0.1, 0.15$, and 0.2) bulk multiferroic ceramics by solution combustion method (SCM). The room temperature magnetic measurement exhibits a weak ferromagnetism and elucidates a superparamagnetic behavior at 5 K of $BiFe_{1-x}Zn_xO_3$ ceramics. The room temperature ferroelectric hysteresis loops of all samples are not really saturated and indicate their ferroelectric nature. A dielectric constant with temperature measurement in $BiFeO_3$, $BiFe_{0.9}Zn_{0.1}O_3$, and $BiFe_{0.85}Zn_{0.15}O_3$ samples exhibits an anomaly around 370, 350, and 300 °C presents an antiferromagnetic to paramagnetic phase transition (T_N).

Acknowledgement

The authors are grateful to UGC-SAP (India) for the support.

References

[1] S.W. Cheong, M. Mostovoy, Nat. Mater. 6 (2007) 13.
[2] N. Kumar, N. Panwar, B. Gahtori, N. Singh, H. Kishan, V.P.S. Awana, J. Alloys Compd. 501 (2010) 129.
[3] V.A Khomchenko, D.A. Kiselev, M. Kopcewicz, M. Maglione, V.V. Shvartsman, P. Borisov, W. Kleemann, A.M.L. Lopes, Y.G. Pogorelov, J.P. Araujo, R.B. Rubinger, N.A. Sobolev, J.M. Vieira, A.L. Kholkin, J. Magn. Magn. Mater. 321 (2009) 1692.
[4] N.A. Spaldin, M. Fiebig, Science 309 (2005) 391.
[5] M. Kumar, K.L. Yadav, Appl. Phys. Lett. 91 (2007) 242901.
[6] F.G. Garcia, C.S. Riccardi, A.Z. Simoes, J. Alloys Compd. 501 (2010) 25.
[7] D. Varshney, A. Kumar, K. Verma, J. Alloys Compd. 509 (2011) 8421.
[8] Y. Wang, J. Alloys Compd. 509 (2011) 1362.
[9] M.Y. Shami, M.S. Awan, M. Anis-ur-Rehman, J. Alloys Compd. 509 (2011) 10139.
[10] A. Azam, A. Jawad, A.S. Ahmed, M. Chaman, A.H. Naqvi, J. Alloys Compd. 509 (2011) 2909.
[11] J. Wei, D. Xue, C. Wu, Z. Lai, J. Alloys Compd. 453 (2008) 20.
[12] X. Zhang, Y. Sui, X. Wang, Y. Wang, Z. Wang, J. Alloys Compd. 507 (2010) 157.
[13] V.R. Reddy, D. Kothari, A. Gupta, S.M. Gupta, Appl. Phys. Lett. 94 (2009) 082505.
[14] D.H. Wang, W.C. Goh, M. Ning, C.K. Ong, Appl. Phys. Lett. 88 (2006) 212907.
[15] Q.H. Jiang, C.W. Nan, Z.J. Shen, J. Am. Ceram. Soc. 89 (7) (2006) 2123.
[16] D.H. Kim, H.N. Lee, M.D. Biegalski, H.M. Christen, Appl. Phys. Lett. 91 (2007) 042906.
[17] M. Kumar, K.L. Yadav, J. Appl. Phys. 100 (2006) 074111.
[18] K.S. Nalwa, A. Garg, A. Upadhyaya, Mater. Lett. 62 (2008) 878.
[19] Q. Xu, H. Zai, D. Wu, Y.K. Tang, M.X. Xu, J. Alloys Compd. 485 (2009) 13.
[20] Y. Wang, G. Xu, L. Yang, Z. Ren, X. Wei, W. Weng, P. Du, G. Shen, G. Han, Mater. Sci. Poland 27 (1) (2009) 219.
[21] D. Kothari, V.R. Reddy, A. Gupta, V. Sathe, A. Banerjee, S.M. Gupta, A.M. Awasthi, Appl. Phys. Lett. 91 (2007) 202505.
[22] S. Chen, L. Wang, H. Xuan, Y. Zheng, D. Wang, J. Wu, Y. Du, Z. Huang, J. Alloys Compd. 506 (2010) 537.
[23] S. Saha, S.J. Ghanawat, R.D. Purohit, J. Mater. Sci. 41 (2006) 1939.
[24] D.P. Dutta, O.D. Jayakumar, A.K. Tyagi, K.G. Girija, C.G.S. Pillai, G. Sharma, Nanoscale 2 (2010) 1149.
[25] V.A. Khomchenko, D.A. Kiselev, J.M. Vieria, A.L. Kholkin, M.A. Sa, Y.G. Pogorelov, Appl. Phys. Lett. 90 (2007) 242901.
[26] D.C. Jia, J.H. Xu, H. Ke, W. Wang, Y. Zhou, J. Eur. Ceram. Soc. 29 (2009) 3099.